APL Bioengineering ARTICLE pubs.aip.org/aip/apb

Single-pericyte nanomechanics measured by contraction cytometry

Cite as: APL Bioeng. **8**, 036109 (2024); doi: 10.1063/5.0213761
Submitted: 12 April 2024 · Accepted: 2 July 2024 ·
Published Online: 9 August 2024

Md. Mydul Islam,[1,2] Ignas Gaska,[3] Oluwamayokun Oshinowo,[1,2] Adiya Otumala,[1,2] Shashank Shekhar,[3] Nicholas Au Yong,[1,4] and David R. Myers[1,2,a)]

AFFILIATIONS

[1]The Wallace H. Coulter Department of Biomedical Engineering, Georgia Institute of Technology & Emory University, Atlanta, Georgia 30332, USA
[2]Department of Pediatrics, Division of Pediatric Hematology/Oncology, Aflac Cancer and Blood Disorders Center of Children's Healthcare of Atlanta, Emory University School of Medicine, Atlanta, Georgia 30322, USA
[3]Departments of Physics, Cell Biology and Biochemistry, Emory University, Atlanta, Georgia 30322, USA
[4]Department of Neurosurgery, Emory University School of Medicine, Atlanta, Georgia 30322, USA

[a)]**Author to whom correspondence should be addressed:** david.myers@emory.edu. **Tel.:** 404-727-0401

ABSTRACT

Pericytes line the microvasculature throughout the body and play a key role in regulating blood flow by constricting and dilating vessels. However, the biophysical mechanisms through which pericytes transduce microenvironmental chemical and mechanical cues to mediate vessel diameter, thereby impacting oxygen and nutrient delivery, remain largely unknown. This knowledge gap is clinically relevant as numerous diseases are associated with the aberrant contraction of pericytes, which are unusually susceptible to injury. Here, we report the development of a high-throughput hydrogel-based pericyte contraction cytometer that quantifies single-cell contraction forces from murine and human pericytes in different microvascular microenvironments and in the presence of competing vasoconstricting and vasodilating stimuli. We further show that murine pericyte survival in hypoxia is mediated by the mechanical microenvironment and that, paradoxically, pre-treating pericytes to reduce contraction increases hypoxic cell death. Moreover, using the contraction cytometer as a drug-screening tool, we found that cofilin-1 could be applied extracellularly to release murine pericytes from hypoxia-induced contractile *rigor mortis* and, therefore, may represent a novel approach for mitigating the long-lasting decrease in blood flow that occurs after hypoxic injury.

INTRODUCTION

The microvasculature comprises the majority of the mammalian cardiovascular system, having an estimated length of >100 000 km in humans.[1] Capillaries—the smallest blood vessels in the microvasculature at 5–10 μm in diameter—are composed of both endothelial cells and pericytes that share a basement membrane of extracellular proteins. At this scale, biophysical interactions between individual cells become important, as red blood cells must squeeze through capillaries to deliver oxygen. Within the microvasculature, pericytes act as living micromechanical gate valves and are the fundamental regulators of microvascular flow[2] [Fig. 1(a)]. Depending on the organ system in which the microvasculature is located, the pericyte-to-endothelial density can be as high as 1:1 (brain) or as low as 1:100 (smooth muscles).[3]

Because pericytes regulate blood flow, their mechanical motions modulate delivery of oxygen and nutrients and even small pericyte contractions and dilations significantly affect the surrounding tissue. For example, one calculation estimated that a 30% constriction of pericytes in the human brain may reduce cerebral blood flow by at least 58%.[4] At the single-cell level, one contracting pericyte can direct blood flow between capillary branches.[5]

Pericytes are unusually susceptible to injury compared to neighboring cells, such as endothelial cells, and numerous diseases are associated with pericyte mechanical dysfunction, including stroke,[6,7] Alzheimer's disease,[4] spinal cord injury,[8] myocardial infarction,[9,10] acute kidney injury,[11] and diabetic retinopathy.[12] Hypoxic environments, such as those occurring in stroke, will induce significant pericyte contraction, followed by cell death and *rigor mortis*, wherein dead pericytes remain contracted, restricting blood flow.[6] As such, hypoxia-induced death and pericyte constriction may exacerbate damage caused by loss of blood flow to an area.[6,7]

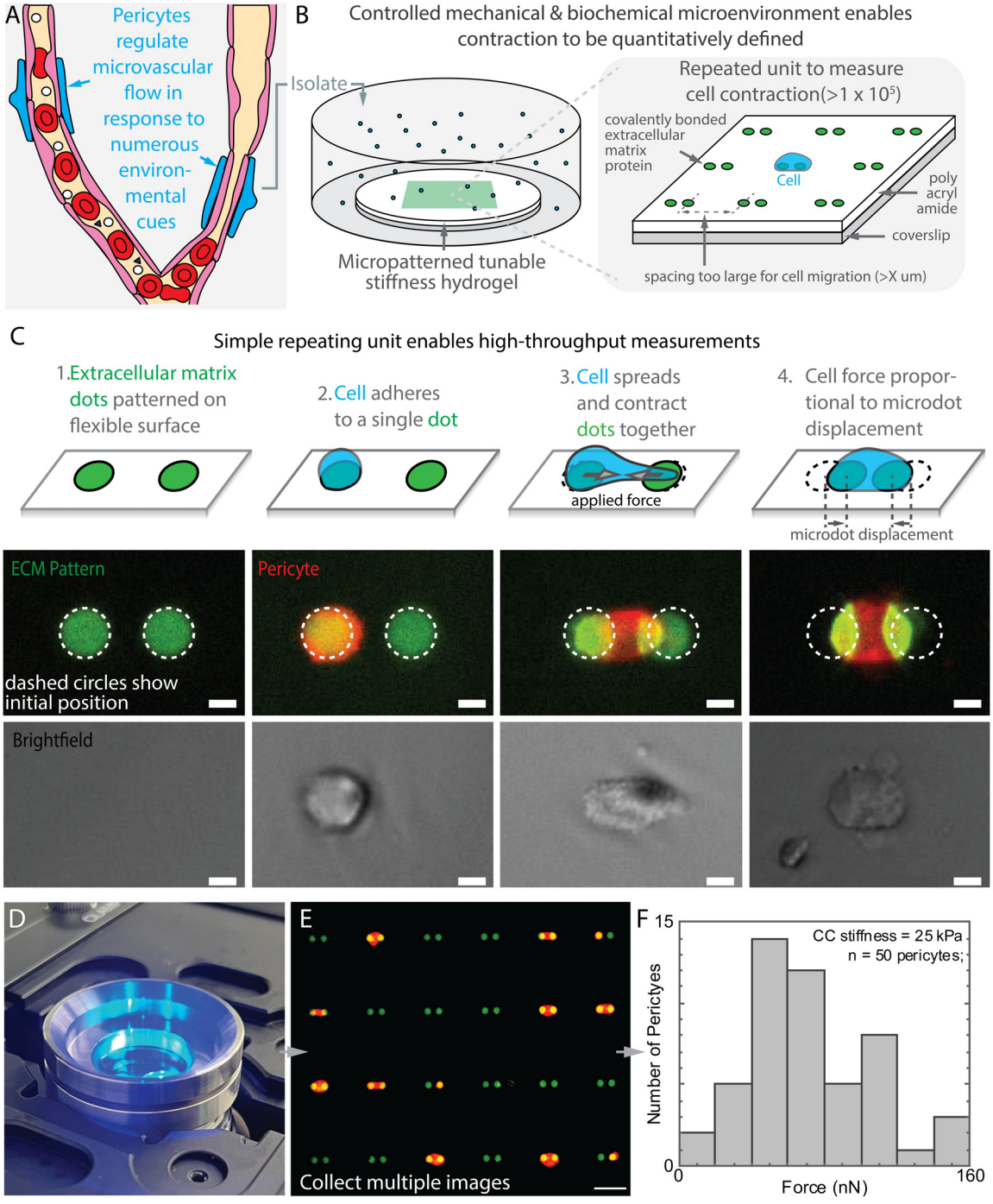

FIG. 1. Contraction cytometry enables high-throughput measurements of single pericytes. (a) Pericytes line the microvasculature and regulate flow in response to environmental cues. (b) By patterning arrays of fluorescently labeled extracellular matrix (ECM) protein dots on polyacrylamide hydrogels, pericyte contraction can be quantitatively measured under well-controlled biochemical and biomechanical conditions. (c) A pericyte will attach, spread, and contract a pair of ECM protein dots. Applied cellular force is directly proportional to the contraction distance. Panels show a pericyte adhering, spreading, and contracting a dot pair. Dashed circles show initial position of microdots. Scale bars, 10 μm. (d) The system is compatible with nearly any epifluorescent scope. (e) Pictures of pericytes on the contraction cytometer are collected and analyzed with a MATLAB script to extract measurements of contraction distance in high throughput. Scale bar, 50 μm. (f) As the mechanics of the system are well defined, contraction distances can also be converted to force; example shows the force of 50 contracting pericytes on a gel stiffness with a of 2.5 kPa.

Despite numerous studies establishing the significance and importance of pericytes in regulating blood flow, due to a dearth of tools, we lack a quantitative understanding of the mechanisms that control and modulate pericyte contraction, both before and after death. Although highly informative, studying pericytes *in vivo* remains time-consuming and limited to select labs with the necessary experience in surgery and imaging procedures. For these analyses, each pericyte's response to stimuli must be measured individually,[4,6,13] and we cannot control the *in vivo* microenvironment, making it difficult to determine quantitative relationships between stimuli and pericyte contraction. Brain slices have similar drawbacks but do not require an animal to be kept alive and sedated during imaging. However, vessels in *ex vivo* tissue are deflated (empty of blood), and the artifacts that may be introduced are still unknown. In contrast, *in vitro* tools, such as wrinkling silicone,[14] micropillar arrays,[15] or bulk collagen gels,[16,17] can measure pericyte contractile biophysics and have provided important insights but are typically low-throughput or non-quantitative.

We developed a novel system for measuring cellular force *in vitro* known as contraction cytometry and extensively validated this method on platelets[18]—anucleate cells that self-assemble and contract to create blood clots.[19] Forces measured from contraction cytometry show high agreement with results from atomic force microscopy[20] and other single-cell force-measurement tools.[21,22] The present work presents the adaption of this system to measuring pericyte nanomechanics. We have extensively optimized our contraction cytometer for pericyte measurements (detailed in "Methods" section). Using this device, we provide quantitative contraction data on >2000 pericytes, the highest number of single-pericyte force measurements to date and, to our knowledge, an order of magnitude higher than any prior work. We also performed an initial study to quantitatively define the force and contractile behavior of single murine and human brain microvascular pericytes in multiple microenvironmental conditions relevant to healthy and pathological conditions.

This work complements a broader effort in the field that seeks to characterize the mechanical properties and behaviors of cell. While our own work focuses on measuring cellular contraction and force, others have helped showcase the importance of measuring cell mechanical properties. A number of excellent reviews have been published that provide details on the underlying determinants of cell mechanical properties, and functional relevance of cell mechanics.[23–25] One ongoing challenge has been that it can be difficult to compare results between different tool types, although important advancements are enabling the ability to measure the mechanical properties of cells using more standardized properties, such as the modulus of elasticity.[26] Such properties are important, as changes in mechanical properties of cells been associated with cancer malignancy,[27,28] chemotherapy,[29] sepsis,[30] phagocytosis,[31,32] and more.

RESULTS

Contraction cytometer measurements align with prior *in vitro* and *in vivo* observations.

Our contraction cytometer is comprised of arrays of micropatterned extracellular matrix (ECM) protein dot pairs covalently attached to a polyacrylamide gel [Fig. 1(b)]. When pericytes are plated and incubated in our system, they attach to a single ECM dot and spread to the neighboring dot; since polyacrylamide is a flexible material, the pericyte can then contract the dots together [Fig. 1(c)]. Moreover, given that the mechanical properties of polyacrylamide are well-defined[33,34] and the stiffness of the microenvironment is known, force can be derived from measurements of the ECM dot area and contraction distance[18] [Figs. 1(d)–1(f)].

To adapt this system for use with pericytes, we empirically optimized the geometry of the measurement system, testing various dot sizes, protein compositions, and spacings. The configuration yielding the highest number of spanning and contracting pericytes had dots composed of collagen, fibronectin, and laminin that were 15 μm in diameter, with a center-to-center distance of 30 μm (supplementary material Fig. 1). This spacing is comparable to the length a pericyte which would cover when encircling a microvessel approximately 9.5 μm in diameter.

To choose the system stiffness, we leveraged prior data and analytical models that were developed by others to define the microenvironmental stiffness of the microvasculature. Early experiments measured dilation of capillaries and venules as a function of pressure, showing capillaries are more rigid than expected.[35] Another early study by Fung *et al.* used a series of analytical models and experimental data of the shear modulus of the mesentery to suggest that vessel stiffness can be derived from local tissue stiffness, comparable to a "tube in a gel" (see supplementary material, Appendix A). Fung *et al.* estimated mesentery to have a shear modulus (G) ranging from 0.3 to 6.0 kg/cm^2 based on experimental measurements. If the Young's modulus (E) is assumed to be $E = 2G(1 + \nu)$, this would correlate with values of 90 kPa–1.8 MPa. Importantly, these values would predict similar vessel dilation in response to pressure as the study showing that capillaries are more rigid than expected.[36] Subsequent vessel dilation and tissue stiffness measurements obtained using more refined tools and techniques estimated a stiffness of 10 kPa.[37] Together, these findings suggest that it is reasonable to estimate microvessel stiffness by considering stiffness of tissue surrounding a hollow tube having the same dimensions as the vessel. In our contraction cytometer, we can approximate this microenvironment by matching the polyacrylamide gel stiffness to that of the tissue in which the pericytes are embedded.

Noting the large number of approximations above and that pericytes regulate blood flow in a variety of tissues, our initial experiments examined pericyte contractile behavior over a range of physiologically relevant stiffnesses (0.25–100 kPa) [Fig. 2(a)]. As expected, results show pericytes are mechanosensitive; resting contraction distance decreased with increasing substrate stiffness, whereas resting "tone" increased with greater stiffness. With some conversion, we are able to compare these results to data obtained from induced pluripotent stem cell (iPS)-derived pericytes on micropillar arrays. On softer arrays (11.6 kPa), pericytes spread on approximately 30 pillars, applying an average of 35 nN per pillar.[15] These values would produce a total applied force of 30×35 nN or approximately 1 μN, which compares favorably with our data [Fig. 2(b)], despite the differing measurement systems. At a micropillar stiffness of 50 kPa, iPS-derived pericytes spread on approximately 200 pillars with an average force of 10 nN per pillar, yielding a total applied force of $\sim$2 μN, which again compares favorably to our estimated force of 1 μN at 50 kPa.[15] Prior work has shown that the total force exerted by a cell on a micropillar array increases linearly with cell area.[38,39] Thus, the slight difference in values may result from the fact that, unlike micropillar arrays, our contraction cytometer imposes a constraint on the pericyte spreading area.

After confirming our system measurements are consistent with those from other *in vitro* tools, we compared pericyte contraction

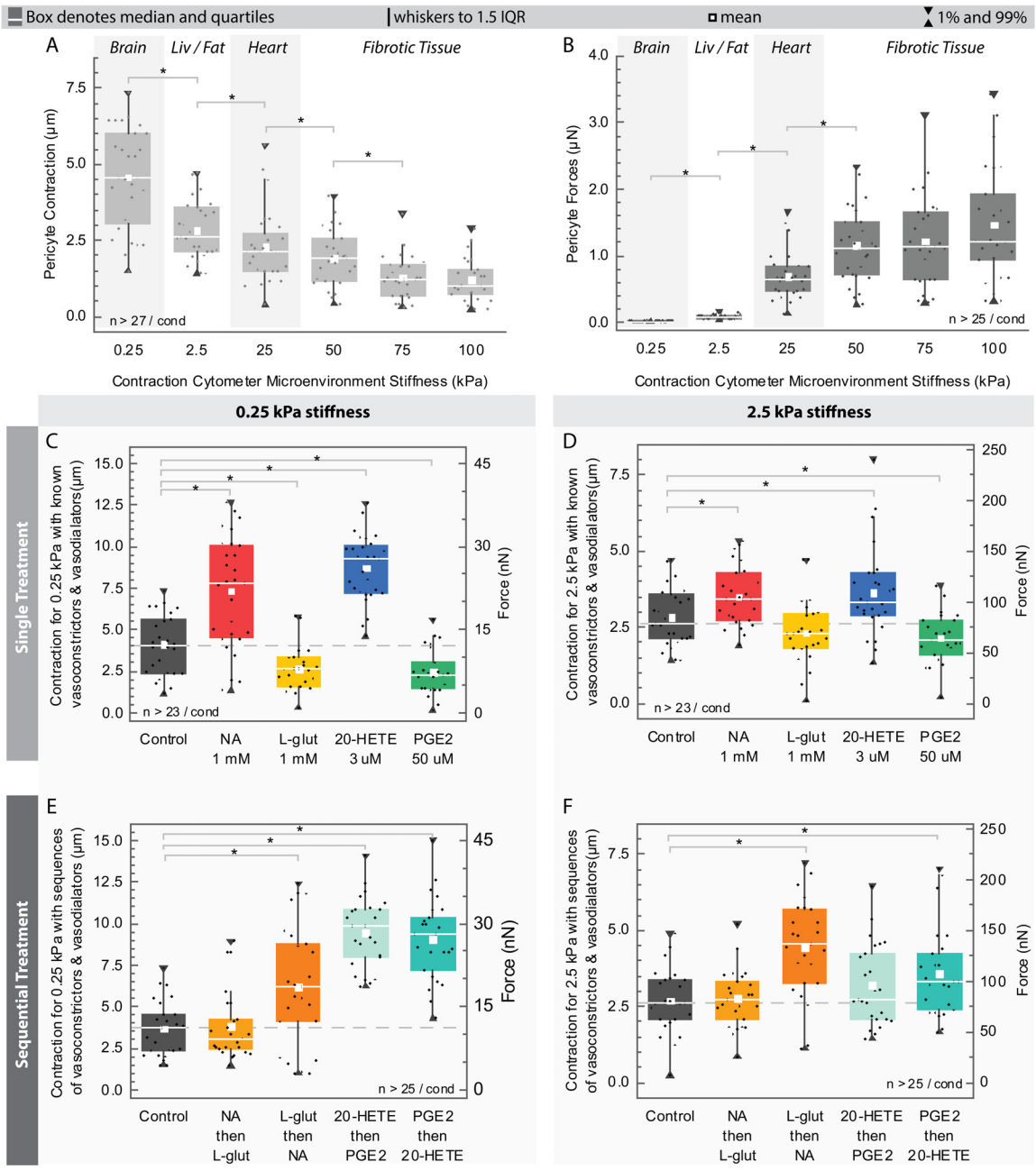

FIG. 2. Pericyte contraction cytometry recapitulates *in vivo* conditions and provides quantitative measurements of contraction distance and force in murine brain microvascular pericytes. (a) Pericytes constrict based on tissue stiffness, contracting more on softer microenvironments. (b) Pericytes apply forces and set a resting tone that increases with increasing tissue stiffness. (c) In stiffnesses associated with healthy brain tissue (0.25 kPa), pericytes contract in response to vasoconstrictors noradrenaline (NA) and 20-hydroxyeicosatetraenoic acid (20-HETE) and relax in response to vasodilators L-glutamine (L-glut) and prostaglandin E2 (PGE2). (d) Pericytes similarly contract and lengthen in stiffnesses associated with brain pathology, albeit with smaller magnitudes. (e) In mixing studies, pericytes were treated with a vasoconstrictor followed by a vasodilator (and vice versa). The observed contractile responses are complex and dependent on the agonist and order of addition. (f) Similar trends were observed in microenvironmental stiffness typical of brain pathology.

cytometry results to *in vivo* observations published by other groups. Given previous models suggesting it is reasonable to assume the surrounding tissue modulates microvessel stiffness and the fact our study focused on brain pericytes, in the remainder of experiments, we used stiffnesses of 0.25 and 2.5 kPa,[40–42] which are specifically relevant to the nervous system. In most *in vivo* studies, pericyte-mediated microvessel contraction was imaged after perfusion with vasoconstrictors and vasodilators. Thus, we plated pericytes and applied noradrenaline

(NA), 20-hydroxyeicosatetraenoic acid (20-HETE), L-glutamate (L-glut), or prostaglandin E2 (PGE2) [Figs. 2(c) and 2(d)]. As expected, pericytes constricted in response to vasoconstrictors (i.e., NA, 20-HETE) and relaxed when treated with vasodilators (L-glut, PGE2). For comparison, a prior report found that *in vivo* pericytes on a 4-μm vessel experienced a 2.5 μm change in diameter in response to NA or a circumference increase in 1.8 μm in response to L-glut (circumference change estimated from vessel diameter).[6] Other vessel diameter measurements in response to varying microenvironmental conditions beyond revealed circumference changes ranging from 1–2 to 12 μm.[7,43] In our system, contraction values at 0.25-kPa stiffness [Fig. 2(c)] more closely match prior published *in vivo* values than those from the 2.5-kPa system [Fig. 2(c)]. Nevertheless, both conditions have value, as stiffer tissue is associated with pathological neurological conditions.[40–42] One important difference between the *in vivo* data of other groups and our *in vitro* data lies in the concentrations of vasoconstrictors and vasodilators needed for comparable contraction or relaxation. For example, the L-glut concentration is comparable to *in vivo* values (0.5 mM),[6] yet the noradrenaline concentrations in our system were much higher than used *in vivo* (2 to 200 μM).[6,44] As has been highlighted previously, NA may modulate more than pericytes and also act on neurons and astrocytes,[6] whereas our system only measures the effects of NA on pericytes alone. Since higher concentrations of NA are needed to stimulate pericyte contraction *in vitro* vs *in vivo*, this supports the idea that NA *in vivo* stimulates pericytes directly while also modulating contraction via other cells.

We next performed a series of sequential-treatment studies aimed at elucidating how pericytes respond to competing vasoconstrictor and vasodilator signals, as might be experienced *in vivo* [Figs. 2(e) and 2(f)]. In these experiments, pericytes were treated with a vasoconstrictor or vasodilator and then treated again in 60 min with a compound in the other group. We obtained highly disparate results depending on the combination of vasoconstrictor and vasodilator tested. For example, with NA and L-glut, pericyte contraction was largely dictated by the second treatment. However, with 20-HETE and PGE2, 20-HETE played a dominant role in signaling regardless of whether the treatment was applied first or second. Although these results are preliminary and do not fully explore this space, they highlight the usefulness of our device of performing quantitative measurements while tightly controlling the microenvironment.

Pericyte response to hypoxia is mechanosensitive

Treatments for ischemic stroke seek to restore blood flow within 4.5 h, as longer timeframes are associated with the no-reflow phenomenon, which occurs when the original obstruction is removed but blood flow is not fully restored.[45] Recent studies by other groups suggest pericytes may underlay this condition, given that when exposed to prolonged hypoxia *in vivo*, these cells constrict, die, and remain in a constricted state after death.[6,7,11,46] Here, we investigated whether pericyte contraction cytometry could be used to study this effect, thereby complementing *in vivo* analyses. We found that pericyte contraction, death, and *rigor mortis* occurred on a contraction cytometer placed in a hypoxic incubator [Figs. 3(a)–3(c)]. Moreover, pericyte death occurred regardless of whether the environment was hypoxic, hypoxic, and ischemic, or hypoxic with inhibition of key metabolic pathways [Fig. 3(d)]. In the latter case, we used iodoacetate plus antimycin to block glycolysis and oxidative phosphorylation, respectively, for comparison with prior studies in which this strategy was utilized to simulate ischemia, albeit under normoxic conditions.[6] As pericytes reside in multicellular networks *in vivo*, our results compare favorably with live imaging of cerebral cortical slices reported earlier by other groups, with some key differences. In cortical slices, 90% of pericytes die after 1 h in simulated chemical ischemia and 40% die in oxygen–glucose-deprivation environments.[6] In our cytometer at 0.25 kPa, 60% and 90% of pericytes expired in 2 and 4 h, respectively, under hypoxic conditions [Figs. 3(d) and 3(e)]. Given that pericytes reside in a complex cellular microenvironment, it is difficult to determine whether pericyte contraction and susceptibility to hypoxia are mediated by external cues or pericyte response to hypoxia. Although our data do not exclude external mediators, they do show that, in response to hypoxia, internal cell processes alone can induce pericyte constriction and death.

Surprisingly, we further found that fewer pericytes died on stiffer substrates (2.5 kPa) at comparable time points [Fig. 3(d)]. To explore this observation, we created contraction cytometers with a variety of stiffnesses and used glass slides for controls. Our data show that substrate stiffness modulates pericyte susceptibility to hypoxic injury, with less cell death occurring on stiffer substrates. Hence, these findings suggest that varying tissue stiffnesses *in vivo* may influence pericyte hypoxic susceptibility. Our data also highlight the drawbacks of using traditional rigid labware and petri dishes to study pericyte response to hypoxia, as such surfaces confer significantly increased protection from hypoxic injury.

We next determined how hypoxia compares to common vasoconstrictors and vasodilators. Overall, we found that hypoxia induced a larger spread in cell-contractile forces [Figs. 3(f) and 3(g)] than NA or L-glut [Figs. 2(c) and 2(d)]. For example, hypoxia induced peak contraction distances of approximately 15 μm in soft gels (0.25 kPa) [Fig. 3(f)], whereas peak distances for NA and L-glut were closer to 12.5 μm [Fig. 2(c)]. However, this increase did not correlate with higher average contraction distances [Figs. 3(f) and 3(g)]. Whereas NA and L-glut induced average contraction changes of about 3.5 and 4.5 μm, respectively, compared to controls [Fig. 2(c)], average contraction distances under hypoxia were approximately 2.0 μm [Fig. 3(f)]. Additionally, the population had a skewed distribution in hypoxic conditions, with many cells experiencing very small to no changes in contractile distance and force; similar trends were also observed on stiffer substrates [Figs. 2(d) and 3(g)].

A key advantage of our system is that it enables biophysical testing and characterization of human brain vascular pericytes that cannot be performed *in vivo*. In our system, we found that human pericytes exhibited biophysical behaviors similar to those of mouse pericytes [Figs. 3(f) and 3(g)], although human cells tended to show a more normal distribution with lower peak maximum-contractile distances.

Pharmacological cytoskeletal inhibition increases hypoxia-induced death

We next investigated the cytoskeletal pathways involved in pericyte response to hypoxia. Pericyte contraction forces are actomyosin mediated[47] and occur after phosphorylation of myosin regulatory light chains, primarily by myosin light chain kinase (MLCK) or Rho-associated protein kinase (ROCK). MLCK phosphorylates myosin light chains. ROCK also phosphorylates myosin light chains leading to contraction, while also inactivating myosin light chain phosphatase,

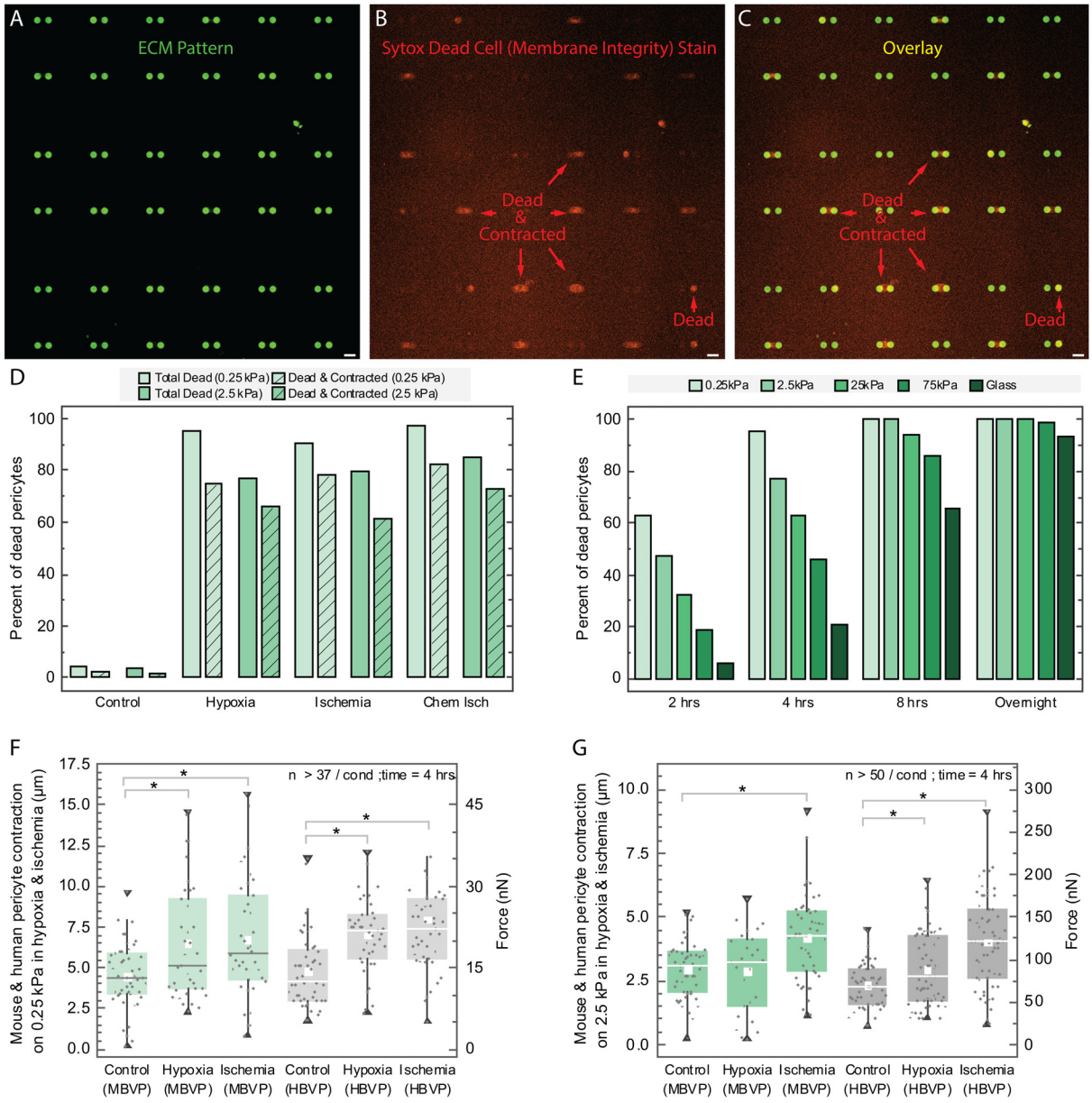

FIG. 3. The mechanical microenvironment influences survivability and contractile response of isolated pericytes to hypoxia. (a)–(c) The contraction cytometer can be readily placed in hypoxic environments, enabling studies of pericyte survivability and contraction. Scalebar 30 μm. (d) Significant death of murine pericytes occurs after exposure to 4 h of hypoxia, hypoxia plus ischemia (zero glucose buffer), or hypoxia plus chemical inhibition (iodoacetate + antimycin), although fewer died in stiffer conditions. (e) Murine pericytes are more susceptible to hypoxic injury and death on softer surfaces and have high survivability on glass. (f) Both murine (green bars) and human (gray bars) brain pericytes constrict under hypoxia; data are from 8 h to ensure all pericytes died. (g) Contractile response is diminished but still present on stiffer (2.5 kPa) substrates.

further promoting contraction.[48] Prior research has shown that, under non-hypoxic conditions, MLCK inhibition reduces contraction *in vitro*.[47] Rho kinase inhibition was further reported to block and even reverse ischemia-induced capillary constriction *in vivo*.[11]

Here, we investigated the importance of these pathways for hypoxia-induced contraction in our system. For this initial analysis, we utilized mouse microvascular brain pericytes, as most prior mechanistic studies have focused on mice or rats.[6,7,11,13,46,49–51] We found that inhibiting MLCK or ROCK with ML-7 or Y-27632, respectively, significantly decreased hypoxia-induced contraction by similar amounts in low and moderate stiffnesses, indicating that both pathways are involved in inducing contraction in the hypoxic cell [Figs. 4(a) and 4(b)]. This finding is consistent with our understanding of hypoxia, wherein catastrophic entry of Ca^{2+} (Ref. 52) can activate MLCK[53] and contraction.

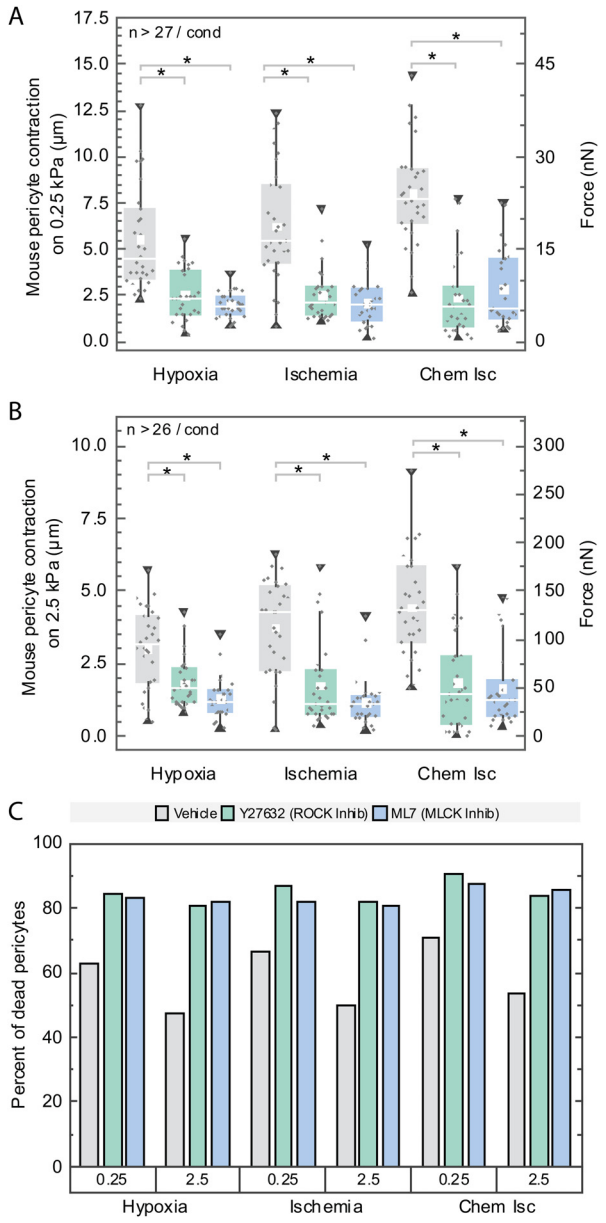

FIG. 4. Inhibiting the Rho-associated protein kinase (ROCK) or myosin light chain kinase (MLCK) pathways reduces contractility while increasing murine pericyte susceptibility to hypoxic death. (a) On soft substrates (0.25 kPa), inhibition of ROCK (via Y-27632) or MLCK (via ML7) signaling decreased contractile distance and force. (b) Similar results were obtained on stiffer substrates at 2.5 kPa. (c) Inhibiting these pathways also increased pericyte susceptibility to hypoxic injury at 2 h.

We further found that impairing murine pericyte contraction via MLCK or ROCK inhibition also significantly increased pericyte susceptibility to hypoxic death [Fig. 4(c)], an interesting observation given that inhibiting cytoskeletal pathways has been proposed as a treatment strategy. Critically, the timing of treatment appears to be important, as ROCK inhibition performed upon reperfusion after injury limited the additional pericyte contraction that accompanies reperfusion and lessened damage to the surrounding tissue (here kidney).[11] Furthermore, administration of fasudil, a Rho kinase inhibiter, to humans 48 h after acute ischemic stroke led to improved neurological function at 2 weeks and clinical outcomes 1 month after the onset of symptoms.[54] It is unclear if these strategies also increase pericyte death, as the pericytes are presumably in hypoxic conditions for shorter times. Thus, although our findings indicate a role for the cytoskeleton in protecting pericytes from hypoxic death *in vitro*, more studies are needed to confirm this phenomenon and determine whether it also occurs in human pericytes.

Cofilin modulates expired pericyte contractility

We next applied our system to assess the potential for modulating postmortem cellular mechanics. If successful, such an approach could release dead cells from *rigor mortis* without increasing pericyte susceptibility to hypoxic injury. The ability to maintain cytoskeletal tension is consistent with our molecular understanding of actomyosin contraction that, specifically, myosin remains stably bound to actin in the absence of ATP.[55] Given our above data showing pericytes remain firmly attached and contracted after expiring from hypoxia [Figs. 3(a)–3(c)], our platform provides an ideal opportunity to measure contractility of dead cells after treatment with various compounds.

We first investigated the effects of cofilin, a well-known cytoskeletal protein that plays multiple roles in actin disassembly.[56–59] Cofilin binds to and severs actin filaments at the interface between cofilin-decorated and bare filament segments and assists with actin network disassembly.[57,58] Decoration of actin filaments by cofilin has also been shown to accelerate depolymerization of actin filaments from their pointed ends.[60,61] We reasoned that re-introducing cofilin would selectively enable cytoskeleton disassembly, although we had several concerns. First, actin severing depends on cofilin levels, optimally occurring at an intermediate concentration. At high concentrations, cofilin saturates actin filaments and prevents fragmentation due to a lack of bare segments. At the molecular level, cofilin induces conformational changes that alter the twist in the actin filaments, and it was also unclear if tensile forces in the cytoskeleton would modulate cofilin actin severing. One study found that tension in actin slows or prevents cofilin severing,[62] whereas another reported that tension can enhance severing.[63] Although all three isoforms of cofilin operate similarly, our studies focused on ubiquitously expressed non-muscle cofilin (cofilin-1).

Immediately prior to necrotic death, hypoxia causes membrane rupture,[52] potentially offering a unique way to specifically target dead and non-living cells. We confirmed this effect in our system and found that, indeed, addition of extracellular cofilin selectively disassembled the actin cytoskeleton of dead murine pericytes [Figs. 5(a)–5(d)], with no effects on living pericytes (1 μM) [Figs. 5(e)–5(h)]. In time-course treatments, dead pericyte cytoskeletons were selectively disassembled by cofilin-1 in approximately 1 h [Figs. 5(d) and 5(h)]. Similar effects were observed in mouse and human pericytes, and, as expected, disassembly decreased with increasing cofilin-1 concentration, particularly between 0.2 and 1 μM [Figs. 5(h)–5(k)]. However, we did not observe a statistically significant difference between 1 and 5 μM, suggesting that any saturation effect was small.

Overall, these results highlight a new potential strategy for treating the no-reflow condition caused by ischemia. Although it is difficult to precisely control concentrations *in vivo*, the broad ability of cofilin-1

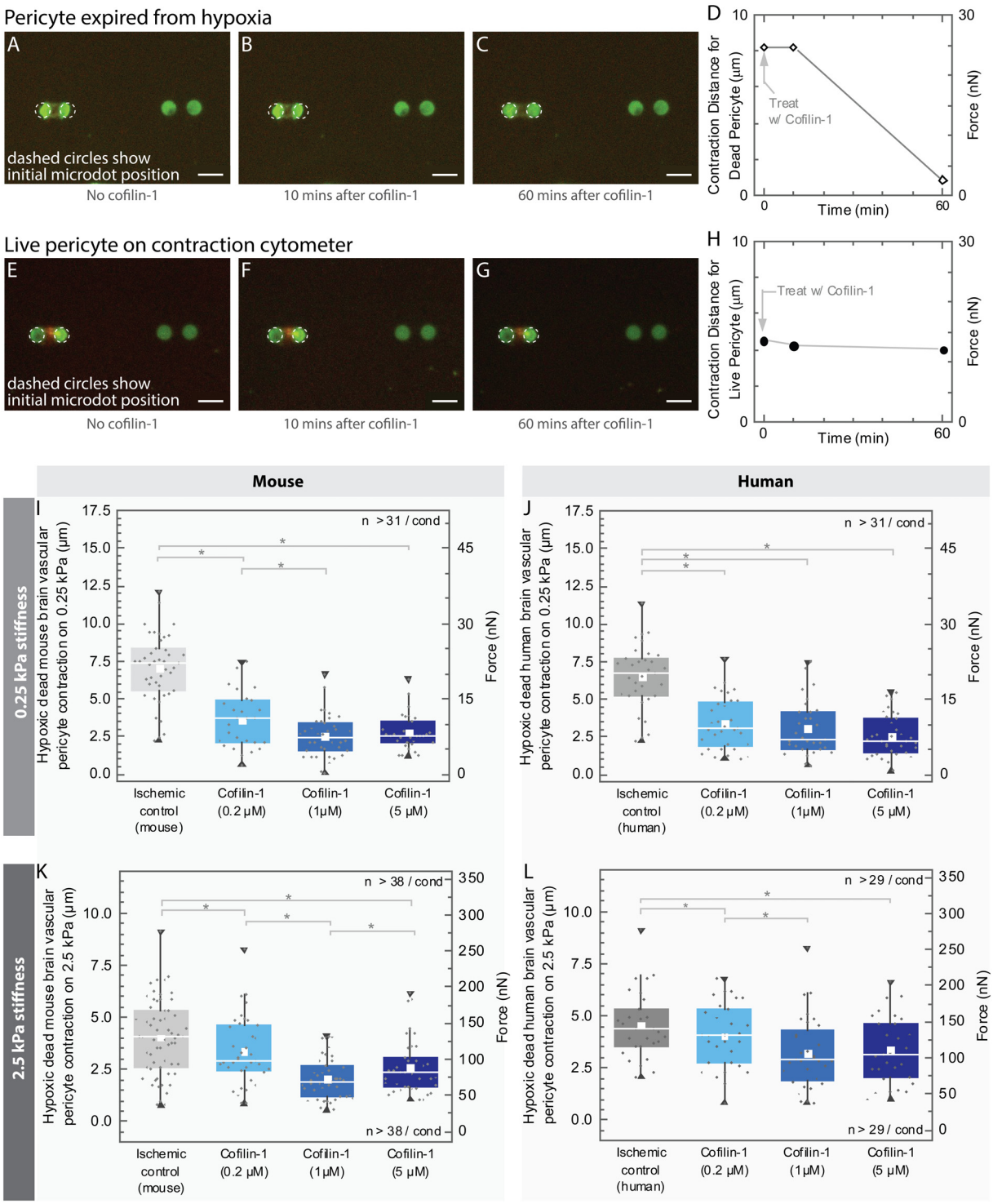

FIG. 5. Treatment with cofilin-1 enables targeted cytoskeleton cleavage in dead murine pericytes. (a)–(d) Pericytes that died from prolonged exposure to hypoxia had their cytoskeletons cleaved by cofilin-1 (1 μM) (e)–(h) whereas living pericytes were unaffected by cofilin-1 treatment (1 μM) and showed no change in contraction over time. Dashed circles show initial position of microdots. Scale bars, 30 μm. (i)–(l) Comparable results were observed in human and mice pericytes under normal (0.25 kPa) and stiff (2.5 kPa) conditions and 1 h of treatment. Final contraction distance was dependent on cofilin-1 concentration, with minor decreases in efficacy observed at higher concentrations.

to promote cytoskeleton severing across a wide range of concentrations suggests the possibility for therapeutic application to reduce contractility in dead cells. Further improvements may also be possible by including other proteins that enhance cofilin-mediated disassembly, such as actin-interacting protein 1[64] (Aip1) and cyclase-associated protein.[65,66] Moreover, our contraction cytometer can be used to screen additional compounds for the ability to modulate dead cell cytoskeletons.

CONCLUSION

Our contraction cytometer has several limitations related to geometry and the multicellular environment. One limitation relates to the quasi-three-dimensional nature of the platform performing high-throughput measurements; rather than constricting a vessel circumferentially, pericytes pull two opposing dots together. Additionally, pericyte interactions and signaling with other cells cannot be easily recapitulated. Instead, this reductionist system excels at identifying pericyte-intrinsic behaviors, which can, in turn, inform thinking on multicellular interactions.

Despite these limitations, our findings demonstrate the potential application of contraction cytometry to study pericyte mechanobiology. After empirical optimization, we validated this platform, showing that pericytes exposed to vasoconstrictors, vasodilators, and hypoxia exhibit similar behaviors as reported *in vivo*. Moreover, by quantitatively measuring pericyte forces and contraction distances in response to varying microenvironmental stimuli, we could compare seemingly disparate conditions. For example, we found hypoxia induces a wider range of contraction forces than vasoconstrictors/vasodilators. We expect that additional such measurements could form the basis for more complex *in silico* simulations to model microvasculature changes in response to varying pathological conditions.

This work also highlights a putative link between hypoxia and the cytoskeleton with possible therapeutic implications, showing that prolonged exposure to hypoxia combined with cytoskeletal targeting increases pericyte susceptibility to hypoxic death. Moreover, by investigating the mechanobiology of dead pericytes, we identified a new possible treatment strategy for selectively targeting and releasing dead pericytes from *rigor mortis*, although an optimal delivery strategy remains to be explored. Finally, our platform simplifies the study of pericyte biophysics, revealing key similarities between biophysical behaviors of human and murine pericytes.

METHODS

Contraction cytometer (PCC) fabrication

The process for contraction cytometer fabrication has been reported previously[18] but is briefly summarized below.

Silicon mold design

The contraction cytometer contains thousands of ECM dot pairs; various geometries of microdot size and center-to-center spacing were created and optimized by maximizing the number of pericytes that spread and contract on the dot pairs. The final design utilized microdots with a diameter of 15 μm and a center-to-center distance of 30 μm. Each microdot pair is 120-μm (horizontally) or 150-μm (vertically) away from the nearest microdot pair neighbor. Our two-dot geometry has been intentionally designed to only allow a pericyte to extend and contract to a neighboring dot while limiting migration due to the large gaps between the dot pairs.

Silicon mold fabrication

Using the aforementioned geometry, a silicon mold was created by standard photolithography and etching to a depth of 800 nm.[18] During cytometer fabrication, the silicon mold is used to remove excess ECM protein from a polydimethylsiloxane (PDMS) stamp, described below, leaving behind protein microdots that can then be transferred to a glass coverslip. When the polyacrylamide gel with cross-liker is incubated on the glass coverslip, the proteins are subsequently transferred. Thus, each hole on the silicon mold will correspond to deposited ECM proteins on the final device.

PDMS micro-stamp preparation

Micro-stamps were fabricated from PDMS, as described previously.[18] Briefly, a thin layer of PDMS was cured in a 100-mm petri dish at a ratio of 10:1 overnight at 60 °C. After curing, the PDMS was cut into approximately 12×12-mm^2 squares and tape-cleaned for ligand stamping.

Ligand stamping on coverslips

Stamped coverslips were prepared using the liftoff method, as described.[18,67] Several potential ligands were assessed, including fluorescently labeled Fibronectin HiLyte 488 (Cat# FNR02-A, Cytoskeleton), Laminin HiLyte 488 (Cat# LMN02-A, Cytoskeleton), DQ^{TM} Collagen, type IV From Human Placenta, Fluorescein Conjugate (Cat# D12052, Thermo Fisher Scientific), and Cocktail (a 1:1:1 mixture of collagen-IV, fibronectin, and laminin ligands). Ligand solutions were incubated onto PDMS micro-stamps at concentrations of 2, 20, 40, and 80 μg/ml for 1 h. Ligand solutions were then rinsed off, and PDMS micro-stamps were cleaned with de-ionized (DI) water and dried with compressed nitrogen. Silicon molds were treated using a Harrick High Powered Expanded Plasma Cleaner (PDC-001-HP) on "high" (45 W) for 60 s. During the treatment, oxygen was flown into the chamber and the pressure was maintained at 0.15 Torr using a Harrick PlasmaFlow PDC-FMG. PDMS micro-stamps were then promptly brought into contact with O_2 plasma-treated silicon molds. After 5 min, PDMS stamps were carefully removed from the mold and transferred onto O_2 plasma-treated 25-mm round coverslips. These coverslips were plasma treated in the same manner as the silicon molds. This step allows transfer of microdot patterns from the PDMS to the O_2 plasma-treated coverslips. However, PDMS micro-stamps were not removed from the patterned coverslips until gel casting was performed under a nitrogen-filled glovebox.

We found that contraction force was statistically similar on the Cocktail of three major ECM proteins encountered in the microvasculature basement membrane (i.e., fibronectin, collagen-IV, laminin) as on fibronectin or collagen, although the Cocktail produced higher contractile-force resting tone than laminin. Additionally, higher concentrations of ECM proteins (40–80 μg/ml) reduced pericyte spreading and force development. We chose to use the protein Cocktail for all our experiments, as this more closely mimics the native ECM.

Coverslip preparation

Prior to hydrogel polymerization, round coverslips (Cat# CLS-1760-025, Chemglass Life Sciences) were treated with a silane solution for 45 min. Silane allows acrylamide gels to attach to the glass surface

and consists of 200-ml DI water, 80-μl acetic acid (Cat# A6283, Sigma), and 50-μl 3-(trimethoxysilyl)propyl methacrylate (Cat# M6514-50mL, Sigma) mixed for 1 h on a magnetic stirrer (Cat# 11-676-265, Thermo Fisher Scientific). The treated sides of coverslips were then thoroughly rinsed with DI water 3–4 times and kept covered with DI water until gel polymerization.

Polyacrylamide gel casting and pattern transfer

Polyacrylamide gels were polymerized onto the Bind Silane–treated coverslips in a nitrogen-filled glovebox (MBraun). Within the glovebox, pre-mixed polyacrylamide solutions were combined with N, N,N′,N′-tetramethylethylenediamine (Cat# T9281, Sigma), 10% ammonium persulfate (Cat# A3678, Sigma), and acrylic acid N-hydroxysuccinimide ester (Cat# A8060, Sigma). Using a 200-μl pipette, 40 μl aliquots of the gel solutions were cast onto the Bind Silane-treated coverslips. Immediately after gel casting, patterned coverslips were removed from PDMS micro-stamps, and the fluorescently labeled, dot-patterned sides of these coverslips were placed on top of the gel-cast coverslips. This step allows both flattening of the polyacrylamide gel and transfer of the ligand-microdot pattern to the polymerized polyacrylamide. Gels were then removed from the glovebox, and the 25-mm round coverslip was carefully removed and discarded. Pattered hydrogels were stored in phosphate-buffered saline (PBS) overnight and for up to 7 days at 4 °C.

PCC device and optimization

The final assembled PCC device consists of thousands of fluorescently labeled microdot arrays covalently bonded to a polyacrylamide gel attached to a glass coverslip mounted on an Attofluor cell chamber (Cat# A7816, Thermo Fisher Scientific).

Experimental methods

Cell culture

Mouse Brain Vascular Pericytes (MBVPs) and Human Brain Vascular Pericytes (HBVPs) were purchased from ScienCell Laboratories and cultured in Pericyte Medium (PM)-mouse (Cat# 1231, ScienCell) or in PM (Cat# 1201, ScienCell), respectively. PM-mouse was supplemented with Pericyte Growth Supplement (PGS)-mouse (Cat# 1282, ScienCell), and PM was supplemented with PGS (Cat# 1252, ScienCell). Both media were also supplemented with fetal bovine serum (Cat# 0010, ScienCell) and Penicillin/Streptomycin Solution (Cat# 0503, ScienCell) to ensure optimal growth and prevent unwanted contamination. Pericytes were grown in six-well cell culture plates coated with poly-L-Lysin (Cat# 0413, ScienCell), according to the manufacturer's instructions for maximum cell growth. Pericytes from passages 5–8 were used for all experiments. For each PCC device, pericytes were seeded at 40×10^4 cells/ml and then incubated at 37 °C and 5% CO_2 for at least 2 h to ensure pericyte attachment on dots. After 2 h, the medium was removed, wells were washed twice with PBS, and fresh medium was added. Pericytes were then grown overnight to achieve more attachment to dots and maximum contraction on dot pairs.

Immunocytochemistry

Depending on the experiment, pericytes were stained with an appropriate plasma membrane dye. To observe pericyte contraction live, PCC samples were incubated in fresh medium supplemented with CellTracker Deep Red Dye (Cat# C34565, ThermoFisher) for 45 min, according to the manufacturer's instructions. PCC samples were then thoroughly washed, and stain-free fresh medium was added. For live contraction observation and post-hypoxic/ischemic experiments, pericytes were stained with a live-cell tracker prior to analyses. For dead pericytes, PCC samples were fixed and stained with 4% paraformaldehyde supplemented with CellMask plasma membrane stain (Cat# C10046, Invitrogen) for 15 min. Samples were then thoroughly washed with PBS and stored in DI water for up to a week. During hypoxia/ischemia experiments, pericyte death was confirmed by supplementing media with SYTOX Dead Cell Stain (Cat# S34859, Thermo Fisher Scientific) at the beginning of the experiment.

Contraction experiments

Pericyte contractility was assessed in our PCC device using a varying degree of hydrogel stiffnesses. In separate experiments, pericytes were exposed to 1-mM of NA (Cat# A7252, Sigma), 3-μM 20-HETE (Cat# 79551-86-3, Cayman Chemical), 1-mM of L-glut (Cat# G5889, Sigma), and 50-μM of PGE2 (Cat# P6532, Sigma) for 1 h. Pericytes were then fixed and stained with an appropriate plasma membrane stain. We also tested the pharmacodynamic effect of two drugs in succession. Briefly, pericytes were incubated with either NA or L-glut for 1 h and washed with PBS to remove any excess compound. Pericytes were then incubated in media supplemented with either L-glut or NA for another hour. In separate experiments, pericytes were incubated first with either 20-HETE or PGE2 for 1 h, washed with PBS, and then incubated either with PGE2 or 20-HETE for an additional hour. At the completion of experiments, pericytes were fixed and stained with a plasma membrane stain and imaged to capture the final contractions.

Hypoxia, ischemia, and chemical ischemia experiments

Hypoxic incubator conditions were generated by replacing the incubator O_2 supply with 95% N_2 and 5% CO_2 for 2 h prior to hypoxia/ischemia experiments. Hypoxia-only conditions were induced by supplementing pericytes with fresh PM and quickly placing them in our hypoxic incubator. For ischemic conditions, pericytes were supplemented with Dulbecco's Modified Eagle Medium (DMEM) lacking glucose (Cat# 11966025, Thermo Fisher Scientific) and placed inside the hypoxic chamber. For chemical ischemia experiments, pericytes were supplemented with DMEM lacking glucose with an additional 2-mM iodoacetate (Cat# I2512, Sigma) and 25-μM antimycin (Cat# A8674, Sigma) to block ATP generation by glycolysis and oxidative phosphorylation, respectively,[6] and then placed inside the hypoxic chamber. In separate experiments, pericytes were incubated with 50-μM ROCK inhibitor Y27632 (Cat# 688001, Millipore Sigma) and 10-μM MLCK inhibitor ML-7 (Cat# BML-EI197-0010, Enzo) prior to assessing contractility under hypoxic and ischemic conditions.

Cofilin-1 experiments

After hypoxic/ischemic pericyte death, growth medium was carefully removed, and PCC samples were supplemented with fresh media containing different concentration of cofilin-1 (i.e., 0.2, 1, 5 μM) for 1 h. PCC samples were then analyzed by live-cell imaging, as described below.

Imaging and mounting

For high-throughput cytometry, gels were imaged on a fluorescent microscope with a 10× objective (Nikon Ti2E Eclipse). For live-cell contraction experiments, PCC samples were mounted on a live-cell on-stage incubator imaging chamber kept at 37 °C and supplemented with 5% CO_2 (Tokai HIT STX Stage Top Incubator). To capture pericyte contraction live, high-resolution images of the samples were obtained with a 20× objective.

Image analysis

Images were analyzed using a custom-written MATLAB script that measured the fluorescent microdot areas and calculated the center0to-center distance of the fluorescent microdots. The uncontracted distance between a dot pair was measured as a reference for comparison with a neighboring dot pair contracted by an individual pericyte. Occasional multi-pericyte aggregates were easily identifiable by size and ignored. Once confocal images were collected, individual pericyte dot pairs were identified by hand and subsequently analyzed by the script.

SUPPLEMENTARY MATERIAL

See the supplementary material for contraction cytometer empirical optimization (Fig. 1) and includes a brief summary of the work of others to estimate capillary mechanics using analytical models and experimental data.

ACKNOWLEDGMENTS

D.R.M. thanks CRD and WAL for helpful conversations. Financial support for this work was provided by a Packard Frontiers in Biosciences and Bioengineering Family Award (MI), an American Society of Hematology Minority Medical Student Award Program Fellowship (OO), The Platelet Disorder Support Association James B. Bussel, MD Young Investigator Award (OO), National Institutes of Health grants (F31HL160210 to OO; K25HL141636 to DRM; R01HL155330 to DRM; and R35GM143050 to SS), and startup funds from Emory University.

AUTHOR DECLARATIONS

Conflict of Interest

M.I., S.S., N.A.Y., and D.R.M. have United States Patent Application No. 63/434/983 pending related to cofilin release of pericytes in rigor mortis.

Ethics Approval

Ethics approval is not required.

Author Contributions

Md Mydul Islam: Investigation (equal); Methodology (equal). **Ignas Gaska:** Resources (supporting). **Oluwamayokun Oshinowo:** Investigation (equal); Methodology (equal). **Adiya Otumala:** Investigation (supporting); Methodology (supporting). **Shashank Shekhar:** Investigation (equal); Resources (supporting); Writing – original draft (supporting). **Nicholas Au Yong:** Conceptualization (equal); Investigation (equal); Supervision (equal). **David R. Myers:** Conceptualization (equal); Funding acquisition (lead); Writing – original draft (equal).

DATA AVAILABILITY

The data that support the findings of this study are openly available in GitHub at https://github.com/davidrmyers/platelet-contraction, Ref. 68.

REFERENCES

[1]M. Feletou, *The Endothelium* (Morgan & Claypool Life Sciences, San Rafael, CA, 2011).
[2]M. E. Kutcher and I. M. Herman, "The pericyte: Cellular regulator of microvascular blood flow," Microvasc. Res. **77**, 235–246 (2009).
[3]S. G. Rayner and Y. Zheng, "Engineered microvessels for the study of human disease," J. Biomech. Eng. **138**, 1108011 (2016).
[4]R. Nortley *et al.*, "Amyloid beta oligomers constrict human capillaries in Alzheimer's disease via signaling to pericytes," Science **365**, eaav9518 (2019).
[5]A. L. Gonzales *et al.*, "Contractile pericytes determine the direction of blood flow at capillary junctions," Proc. Natl. Acad. Sci. U. S. A. **117**, 27022–27033 (2020).
[6]C. N. Hall *et al.*, "Capillary pericytes regulate cerebral blood flow in health and disease," Nature **508**, 55–60 (2014).
[7]M. Yemisci *et al.*, "Pericyte contraction induced by oxidative-nitrative stress impairs capillary reflow despite successful opening of an occluded cerebral artery," Nat. Med. **15**, 1031–1037 (2009).
[8]Y. Li *et al.*, "Pericytes impair capillary blood flow and motor function after chronic spinal cord injury," Nat. Med. **23**, 733–741 (2017).
[9]C. Methner, Z. Cao, A. Mishra, and S. Kaul, "Mechanism and potential treatment of the 'no reflow' phenomenon after acute myocardial infarction: Role of pericytes and GPR39," Am. J. Physiol.: Heart Circ. Physiol. **321**, H1030 (2021).
[10]I. G. Rolle *et al.*, "Heart failure impairs the mechanotransduction properties of human cardiac pericytes," J. Mol. Cell. Cardiol. **151**, 15–30 (2021).
[11]F. Freitas and D. Attwell, "Pericyte-mediated constriction of renal capillaries evokes no-reflow and kidney injury following ischaemia," eLife **11**, e74211 (2022).
[12]H.-P. Hammes *et al.*, "Pericytes and the pathogenesis of diabetic retinopathy," Diabetes **51**, 3107–3112 (2002).
[13]N. Korte *et al.*, "The Ca^{2+}-gated channel TMEM16A amplifies capillary pericyte contraction and reduces cerebral blood flow after ischemia," J. Clin. Invest. **132**, e154118 (2022).
[14]M. Kotecki, A. S. Zeiger, K. J. Van Vliet, and I. M. Herman, "Calpain- and talin-dependent control of microvascular pericyte contractility and cellular stiffness," Microvasc. Res. **80**, 339–348 (2010).
[15]O. Iendaltseva, V. V. Orlova, C. L. Mummery, E. H. J. Danen, and T. Schmidt, "Fibronectin patches as anchoring points for force sensing and transmission in human induced pluripotent stem cell-derived pericytes," Stem Cell Rep. **14**, 1107–1122 (2020).
[16]C. L. Speyer, C. P. Steffes, and J. L. Ram, "Effects of vasoactive mediators on the rat lung pericyte: Quantitative analysis of contraction on collagen lattice matrices," Microvasc. Res. **57**, 134–143 (1999).
[17]C. Kelley, P. D'Amore, H. B. Hechtman, and D. Shepro, "Microvascular pericyte contractility in vitro: Comparison with other cells of the vascular wall," J. Cell Biol. **104**, 483–490 (1987).
[18]D. R. Myers *et al.*, "Single-platelet nanomechanics measured by high-throughput cytometry," Nat. Mater. **16**, 230–235 (2017).

[19]Y. Qiu, D. R. Myers, and W. A. Lam, "The biophysics and mechanics of blood from a materials perspective," Nat. Rev. Mater. **4**, 294–311 (2019).
[20]W. A. Lam *et al.*, "Mechanics and contraction dynamics of single platelets and implications for clot stiffening," Nat. Mater. **10**, 61–66 (2011).
[21]M. Y. Mollica *et al.*, "Distinct platelet F-actin patterns and traction forces on von Willebrand factor versus fibrinogen," Biophys. J. **122**, 3738–3748 (2023).
[22]K. M. Beussman *et al.*, "Black dots: High-yield traction force microscopy reveals structural factors contributing to platelet forces," Acta Biomater. **163**, 302–311 (2021).
[23]M. Urbanska and J. Guck, "Single-cell mechanics: Structural determinants and functional relevance," Annu. Rev. Biophys. **53**, 367–395 (2024).
[24]H. Chen, J. Guo, F. Bian, and Y. Zhao, "Microfluidic technologies for cell deformability cytometry," Smart Med. **1**, e20220001 (2022).
[25]B. N. Narasimhan *et al.*, "Mechanical characterization for cellular mechanobiology: Current trends and future prospects," Front. Bioeng. Biotechnol. **8**, 595978 (2020).
[26]A. Abarca-Ortega *et al.*, "Single-cell mechanical characterization in constriction-based cytometry," Int. J. Mech. Sci. **268**, 108979 (2024).
[27]H. T. K. Tse *et al.*, "Quantitative diagnosis of malignant pleural effusions by single-cell mechanophenotyping," Sci. Transl. Med. **5**, 212ra163 (2013).
[28]J. Guck *et al.*, "Optical deformability as an inherent cell marker for testing malignant transformation and metastatic competence," Biophys. J. **88**, 3689–3698 (2005).
[29]W. A. Lam, M. J. Rosenbluth, and D. A. Fletcher, "Chemotherapy exposure increases leukemia cell stiffness," Blood **109**, 3505–3508 (2006).
[30]K. Crawford *et al.*, "Rapid biophysical analysis of host immune cell variations associated with sepsis," Am. J. Respir. Crit. Care Med. **198**, 280–282 (2018).
[31]N. G. Sosale *et al.*, "Cell rigidity and shape override CD47's 'self'-signaling in phagocytosis by hyperactivating myosin-II," Blood **125**, 542–552 (2015).
[32]I. Pushkarsky *et al.*, "Elastomeric sensor surfaces for high-throughput single-cell force cytometry," Nat. Biomed. Eng. **2**, 124–137 (2018).
[33]J. R. Tse and A. J. Engler, "Preparation of hydrogel substrates with tunable mechanical properties," Curr. Protoc. Cell Biol. **47**, 10.16.1–10.16.16 (2010).
[34]A. K. Denisin and B. L. Pruitt, "Tuning the range of polyacrylamide gel stiffness for mechanobiology applications," ACS Appl. Mater. Interfaces **8**, 21893–21902 (2016).
[35]S. Baez, H. Lamport, and A. Baez, "Pressure effects in living microscopic vessels," in *Flow Properties of Blood* (American Heart Association, 1960).
[36]Y. C. Fung, B. W. Zweifach, and M. Intaglietta, "Elastic environment of the capillary bed," Circ. Res. **19**, 441–461 (1966).
[37]L. H. Smaje, P. A. Fraser, and G. Clough, "The distensibility of single capillaries and venules in the cat mesentery," Microvasc. Res. **20**, 358–370 (1980).
[38]D. W. Dumbauld *et al.*, "How vinculin regulates force transmission," Proc. Natl. Acad. Sci. U. S. A. **110**, 9788–9793 (2013).
[39]E. N. Holland, D. Lobaccaro, J. Fu, and A. J. García, "Impact of adhesive area on cellular traction force and spread area," J. Biomed. Mater. Res., Part A **111**, 609–617 (2023).
[40]K. M. Stroka and H. Aranda-Espinoza, "Endothelial cell substrate stiffness influences neutrophil transmigration via myosin light chain kinase-dependent cell contraction," Blood **118**, 1632–1640 (2011).
[41]M. Khoonkari, D. Liang, M. Kamperman, F. A. E. Kruyt, and P. van Rijn, "Physics of brain cancer: Multiscale alterations of glioblastoma cells under extracellular matrix stiffening," Pharmaceutics **14**, 1031 (2022).
[42]B. Deng *et al.*, "Biological role of matrix stiffness in tumor growth and treatment," J. Transl. Med. **20**, 540 (2022).
[43]C. M. Peppiatt, C. Howarth, P. Mobbs, and D. Attwell, "Bidirectional control of CNS capillary diameter by pericytes," Nature **443**, 700–704 (2006).
[44]N. Korte *et al.*, "Noradrenaline released from locus coeruleus axons contracts cerebral capillary pericytes via α2 adrenergic receptors," J. Cereb. Blood Flow Metab. **43**, 1142–1152 (2023).
[45]D. M. Greif and A. Eichmann, "Brain vessels squeezed to death," Nature **508**, 50–51 (2014).
[46]M. A. Costa *et al.*, "Pericytes constrict blood vessels after myocardial ischemia," J. Mol. Cell. Cardiol. **116**, 1–4 (2018).
[47]S. Lee *et al.*, "Pericyte actomyosin-mediated contraction at the cell–material interface can modulate the microvascular niche," J. Phys.: Condens. Matter **22**, 194115 (2010).
[48]O. A. Kazakova, A. Y. Khapchaev, and V. P. Shirinsky, "MLCK and ROCK mutualism in endothelial barrier dysfunction," Biochimie **168**, 83–91 (2020).
[49]D. A. Hartmann *et al.*, "Brain capillary pericytes exert a substantial but slow influence on blood flow," Nat. Neurosci. **24**, 633–645 (2021).
[50]K. Oishi, T. Kamiyashiki, and Y. Ito, "Isometric contraction of microvascular pericytes from mouse brain parenchyma," Microvasc. Res. **73**, 20–28 (2007).
[51]F. M. O'Farrell *et al.*, "Capillary pericytes mediate coronary no-reflow after myocardial ischaemia," eLife **6**, e29280 (2017).
[52]R. G. Boutilier, "Mechanisms of cell survival in hypoxia and hypothermia," J. Exp. Biol. **204**, 3171–3181 (2001).
[53]K. Suzuki-Inoue *et al.*, "Involvement of Src kinases and PLCγ2 in clot retraction," Thromb. Res. **120**, 251–258 (2007).
[54]M. Shibuya *et al.*, "Effects of fasudil in acute ischemic stroke: Results of a prospective placebo-controlled double-blind trial," J. Neurol. Sci. **238**, 31–39 (2005).
[55]I. Pepper and V. E. Galkin, "Actomyosin complex," Subcell. Biochem. **99**, 421–470 (2022).
[56]P. Lappalainen and D. G. Drubin, "Cofilin promotes rapid actin filament turnover *in vivo*," Nature **388**, 78–82 (1997).
[57]B. L. Goode, J. Eskin, and S. Shekhar, "Mechanisms of actin disassembly and turnover," J. Cell Biol. **222**, e202309021 (2023).
[58]P. Lappalainen, T. Kotila, A. Jégou, and G. Romet-Lemonne, "Biochemical and mechanical regulation of actin dynamics," Nat. Rev. Mol. Cell Biol. **23**, 836–852 (2022).
[59]P. Lappalainen and D. G. Drubin, "Cofilin promotes rapid actin filament turnover *in vivo*," Nature **389**, 211–211 (1997).
[60]S. Shekhar and M.-F. Carlier, "Enhanced depolymerization of actin filaments by ADF/cofilin and monomer funneling by capping protein cooperate to accelerate barbed-end growth," Curr. Biol. **27**, 1990–1998.E5 (2017).
[61]H. Wioland *et al.*, "ADF/cofilin accelerates actin dynamics by severing filaments and promoting their depolymerization at both ends," Curr. Biol. **27**, 1956–1967.E7 (2017).
[62]K. Hayakawa, H. Tatsumi, and M. Sokabe, "Actin filaments function as a tension sensor by tension-dependent binding of cofilin to the filament," J. Cell Biol. **195**, 721–727 (2011).
[63]H. Wioland, A. Jegou, and G. Romet-Lemonne, "Torsional stress generated by ADF/cofilin on cross-linked actin filaments boosts their severing," Proc. Natl. Acad. Sci. U. S. A. **116**, 2595–2602 (2019).
[64]K. Okada, H. Ravi, E. M. Smith, and B. L. Goode, "Aip1 and Cofilin promote rapid turnover of yeast actin patches and cables: A coordinated mechanism for severing and capping filaments," Mol. Biol. Cell **17**, 2855–2868 (2006).
[65]S. Shekhar, J. Chung, J. Kondev, J. Gelles, and B. L. Goode, "Synergy between Cyclase-associated protein and Cofilin accelerates actin filament depolymerization by two orders of magnitude," Nat. Commun. **10**, 5319 (2019).
[66]T. Kotila *et al.*, "Mechanism of synergistic actin filament pointed end depolymerization by cyclase-associated protein and cofilin," Nat. Commun. **10**, 5320 (2019).
[67]A. C. von Philipsborn *et al.*, "Microcontact printing of axon guidance molecules for generation of graded patterns," Nat. Protoc. **1**, 1322–1328 (2006).
[68]M. Fay and D. Myers (2016). "MATLAB script to analyze contraction cytometer," GitHub. https://github.com/davidrmyers/platelet-contraction